Applied Environmental Research (2026) 48(3), 019
https://doi.org/10.35762/AER.2026019

Applied Environmental Research
- RESEARCH FOR SUSTAINABLE PLANET -

Research Article

Spatial Modeling of Natural Disaster Risk by Integrating Hazard, Vulnerability, and Exposure Factors using Geospatial Techniques: Evidence from Mueang Tak District, Thailand

Suphatphong Ruthamnong*

Kamphaeng Phet Rajabhat University

*Corresponding Email: suphatphong007@hotmail.com

Abstract

This study presents a comprehensive multihazard risk assessment for Mueang Tak District, Thailand, that integrates hazard, vulnerability, and exposure (H-V-E) dimensions. By utilizing geographic information systems (GIS) and remote sensing, the analytic hierarchy process (AHP) was employed to prioritize critical risk factors. GIS analysis integrated multisource spatial data, including Landsat 9 and Sentinel-2 imagery, CHIRPS precipitation, and SRTM-derived topography, while AHP weights were established on the basis of expert judgment and socioeconomic indices such as the relative wealth index (RWI) and population statistics. The results delineate distinct spatial risk clusters: high landslide potential is concentrated in the steep terrain of Mae Tho subdistrict, critical flood exposure affects the urbanized lowlands of Tak Municipality, and severe drought vulnerability characterizes the rain-fed agricultural belts of Pa Mamuang and Wang Prachop. These spatially explicit findings demonstrate the robustness of the integrated geospatial model, providing essential data to guide local policymakers in establishing “Disaster Risk Reduction Sandbox” areas and enhancing community resilience against compounding natural hazards.

ARTICLE HISTORY

Received: 14 Dec. 2025
Revised: 12 Mar. 2026
Accepted: 13 Mar. 2026
Published: 9 Apr. 2026

KEYWORDS

Disaster risk assessment;
Geographic information system (GIS);
Analytic hierarchy process (AHP);
Landslide;
Flood;
Drought

Introduction

Natural disasters, including landslides, floods, and droughts, pose significant threats to human security, economic stability, and environmental sustainability globally. Recently, the frequency and intensity of these events have increased due to climate change and anthropogenic factors, necessitating effective disaster risk reduction (DRR) strategies (Aldiansyah et al., 2025). Risk assessment is a fundamental component of mitigation, providing essential data for planning and decision-making. The concept of risk is generally defined as a function of hazard, vulnerability, and exposure. Understanding the spatial distribution of these components is crucial for identifying high-risk zones and prioritizing management efforts (Mulabbi et al., 2025).

Geospatial technologies, specifically geographic information systems (GIS) and remote sensing (RS), have become indispensable tools for natural hazard analysis. They allow for the efficient integration and processing of multi-source spatial data to model complex environmental phenomena. Among various methodologies, the analytic hierarchy process (AHP) and index-based models are widely recognized for their effectiveness in evaluating disaster susceptibility (Alamrew et al., 2024; Kayastha et al., 2013; Pourghasemi et al., 2012; Yalcin et al., 2008). Previous studies have successfully applied these techniques to map flood risks in large river basins by integrating hydrological and geomorphological factors (Al Ali et al., 2023; Selvam and Jebamalai, 2023), as well as landslide susceptibility through the analysis of slope, lithology,

and land cover (Alamrew et al., 2024; Kayastha et al., 2013; Muhimbula et al., 2025; Pourghasemi et al., 2012). Similarly, drought risk assessments have increasingly adopted index-based approaches using satellite-derived data to monitor agricultural sensitivity and potential impacts on economic crops (Alharbiet al., 2022; de Azevedo Reis et al., 2020; Kukuntod and Wijitkosum, 2025).

Despite the advancements in hazard modeling, many studies focus on single-hazard assessments or primarily on the physical aspect (hazard) while overlooking the socio-economic dimensions of vulnerability and exposure. Furthermore, in the context of Thailand, specifically in Mueang Tak District, there is a lack of comprehensive multi-hazard risk assessments that integrate hazard, vulnerability, and exposure dimensions at a local scale. Mueang Tak District is characterized by diverse topography, ranging from mountainous terrain prone to landslides to low-lying floodplains along the Ping River, and rain-fed agricultural areas susceptible to drought. The existing disaster management approach in the area often operates in silos, lacking an integrated spatial database to support holistic planning and community-based solutions.

To address these gaps, this study aims to analyze and map the risk areas for three major natural disasters—landslides, floods, and droughts—in Mueang Tak District. The research adopts an integrated framework that combines hazard, vulnerability, and exposure factors using GIS and Remote Sensing techniques. The specific objectives are to identify spatial risk patterns and determine the relative importance of conditioning factors through the AHP method. The findings of this study are intended to provide a scientific basis for local authorities to develop targeted mitigation strategies and support the establishment of disaster risk management innovation areas.

Materials and methods

1) Study area

This study focuses on Mueang Tak District, which serves as the administrative center of Tak Province in the western region of Thailand. The district covers an area of approximately 159,936 ha, accounting for 9.75% of the province's total area. This area is located between 16°33' and 17°12' north latitude and 98°49' and 99°28' east longitude (Figure 1). Administratively, the district is divided into 11 local administrative units, comprising Tak Municipality (TM) and 10 subdistricts: Nong Bua Nuea (NBN), Mai Ngam (MNG), Pong Daeng (PD), Nam Ruem (RM), Wang Hin (WH), Mae Tho (MT), Pa Mamuang (PMM), Nong Bua Tai (NBT), Wang Prachop (WPC), and Taluk Klang Thung (TKT). Geographically, the district is situated along the Ping River, which serves as the main water resource and flows from north to south through the area (Department of Provincial Administration, 2024).

The topography is diverse and complex, ranging from low-lying alluvial plains to rugged high mountain ranges. The elevation varies significantly from 91 to 1,190 meters above mean sea level (mamsl), with slope gradients ranging from flat terrain in the eastern river basins to steep slopes exceeding 45 degrees in the western mountainous zones. With respect to land use and land cover (LULC), more than 60.93% of the district is covered by forestland areas, primarily in the highlands. Agricultural land represents the second-largest category, where cassava and rice are the dominant economic crops. The soil characteristics are predominantly complex slope soils in the highlands and sandy loam in the lowlands (Department of Provincial Administration, 2024; Kamphaeng Phet Rajabhat University, 2018; Ruthamnong et al., 2023).

The climate of Mueang Tak District is classified as a tropical savanna climate (Köppen climate classification Aw) (Office of the Permanent Secretary, Ministry of Agriculture and Cooperatives, 2025). The area experiences an average annual rainfall of approximately 1,255 mm, with the highest precipitation occurring in September because of the influence of the southwest monsoon (Weather Spark, 2025).

This distinct topographical and climatic setting exposes the district to multiple natural hazards. The low-lying communities along the Ping River banks, particularly in Tak Municipality, are frequently subjected to riverine flooding during the monsoon season because of limited drainage capacity. In contrast, the steep mountainous areas in subdistricts such as Mae Tho are highly susceptible to landslides and flash floods triggered by heavy rainfall. Conversely, rain-fed agricultural zones outside the irrigation network, such as those in the Wang Prachop and Taluk Klang Thung subdistricts, often face severe drought conditions during the dry season, impacting crop production and local livelihoods (The Nation Thailand, 2025).

2) Methodological framework

To address the variability in risk assessment standards, this study adopts a specific geospatial multi-criteria framework derived from the United Nations Office for Disaster Risk Reduction (UNDRR) guidelines (IPCC, 2012; United Nations General Assembly, 2016). The conceptual workflow, illustrating the partition and interaction between dimensions, is presented in Figure 2. To minimize functional overlap, the risk components are rigorously partitioned as follows:

- Hazard (H): This term refers to the physical probability and magnitude of the natural event (e.g., slope gradient or rainfall intensity) that acts as the trigger.

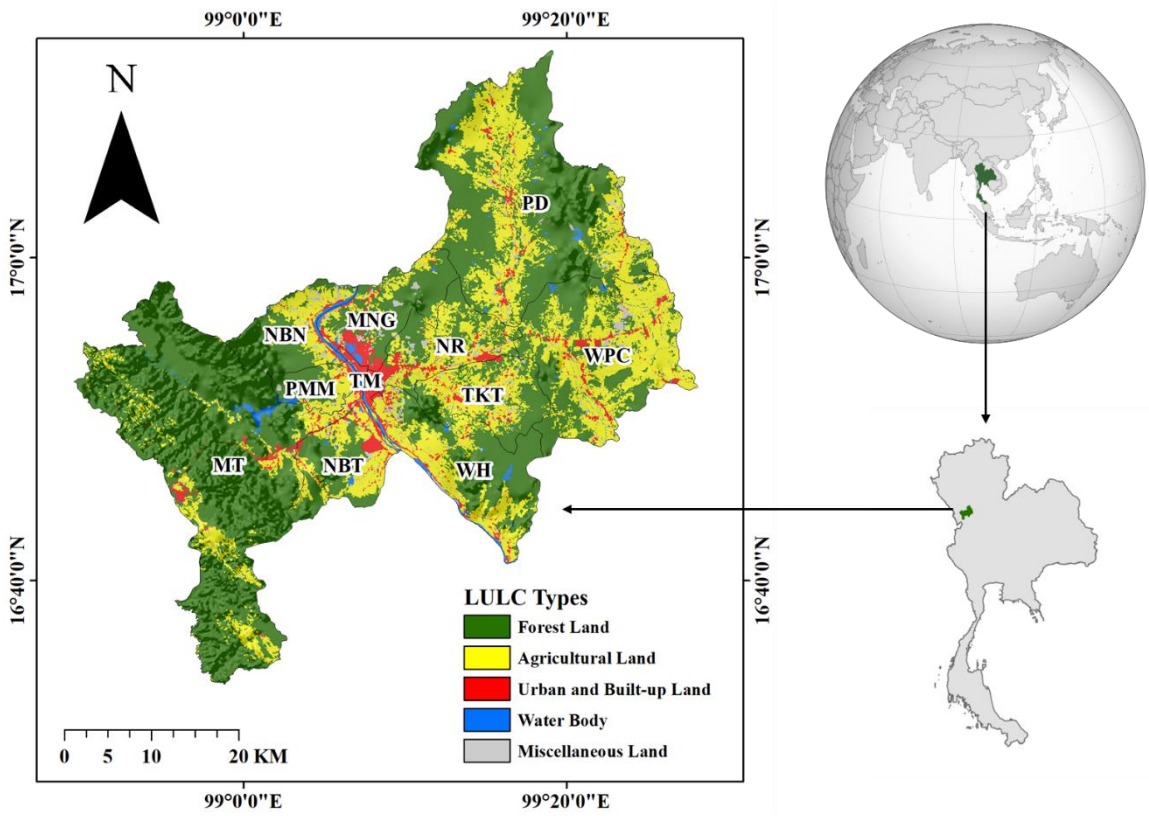

Figure 1 Map of the research locations.

- Vulnerability (V): This represents the intrinsic susceptibility of the community or environment to damage (e.g., poverty levels via RWI or lack of drainage capacity) and focuses on the “quality” or “condition” of the area.

- Exposure (E): Denotes the presence of elements at risk—specifically, the spatial density of built-up areas and agricultural assets—focusing strictly on the “quantity” of assets subject to potential losses.

The research workflow is illustrated in Figure 2. The process is structured into four distinct phases: (1) Data acquisition & preparation, involving the collection of satellite imagery and ancillary data, followed by pre-processing and standardization via min–max normalization; (2) criteria analysis, where conditioning factors are categorized under the hazard-vulnerability-exposure (H-V-E) framework; (3) risk modeling, which uses the AHP for weighting and weighted linear combination (WLC) for spatial integration; and (4) validation, which employs statistical validation techniques to verify the accuracy of the multihazard risk maps against ground-truth data.

3) Data collection and interpretation

To comprehensively assess multihazard risks, this study integrated multisource geospatial data, including satellite imagery, climate data, and socioeconomic statistics. The data collection and interpretation process was primarily conducted using the Google Earth Engine (GEE) for the cloud-based processing of large datasets (Gorelick et al., 2017) and the QGIS (Quantum GIS) for vector and raster analysis and map production.

Remote sensing data: Satellite imagery was acquired via GEE to derive key environmental indices. Landsat 9 OLI-2/TIRS-2 imagery (February 2025) and Sentinel-2 time series data (2020–2024) were used to analyze land use/land cover (LULC) and compute vegetation indices such as the normalized difference vegetation index (NDVI) and vegetation health index (VHI). Precipitation data were derived from the Climate Hazards Group InfraRed Precipitation with Station data (CHIRPS Daily) (Funk et al., 2015) and processed to obtain the current year and annual average precipitation layers. Topographical features, including elevation, slope, and the topographic wetness index (TWI), were extracted from the Shuttle Radar Topography Mission (SRTM) digital elevation model (DEM) at a 30-meter resolution. Additionally, the Visible Infrared Imaging Radiometer Suite (VIIRS) Nighttime Lights dataset (Elvidge et al., 2017) and Global Human Settlement Layer (GHSL) (Pesaresi et al., 2013) were used to assess urbanization and impervious surface fractions (ISF).

GIS and ancillary data: Vector data layers representing physical and social infrastructure were collected from relevant Thai government agencies. These included administrative boundaries, soil texture, geological faults, road networks, and irrigation zones, sourced from the Land Development Department (LDD), Royal Irrigation Department (RID), and the Department of Mineral Resources (DMR), respectively. Demographic data, specifically population density and household statistics

(2024), were obtained from the National Statistical Office (NSO) to evaluate social vulnerability. To assess economic vulnerability, the relative wealth index (RWI) was utilized. The RWI is a high-resolution grid (2.4 km) developed by Meta that predicts the relative standard of living within a country using machine learning models trained on connectivity data, satellite imagery, and demographic surveys. This index serves as a validated proxy for household economic stability (Chi et al., 2022). The detailed specifications of these multisource datasets, including their data providers, acquisition dates, and original spatial resolutions, are summarized in Table 1.

Data Preprocessing: To ensure spatial consistency for the multi-criteria decision analysis (MCDA), all vector and raster datasets were projected to the WGS 1984 UTM Zone 47 N coordinate system. Raster datasets were resampled to a unified spatial resolution of 20 meters. This intermediate scale was chosen to bridge the gap between fine-scale Sentinel-2 imagery (10 m) and coarser topographical inputs (30 m), balancing the preservation of spectral details with the limitations of downscaling uncertainty. This resolution is considered optimal for identifying strategic risk clusters at the district planning level. A min–max normalization method was subsequently applied to transform all the data values into a standardized range of 0 to 1, facilitating the integration of factors with different units (e.g., rainfall in mm vs. slope in degrees) into the risk assessment model.

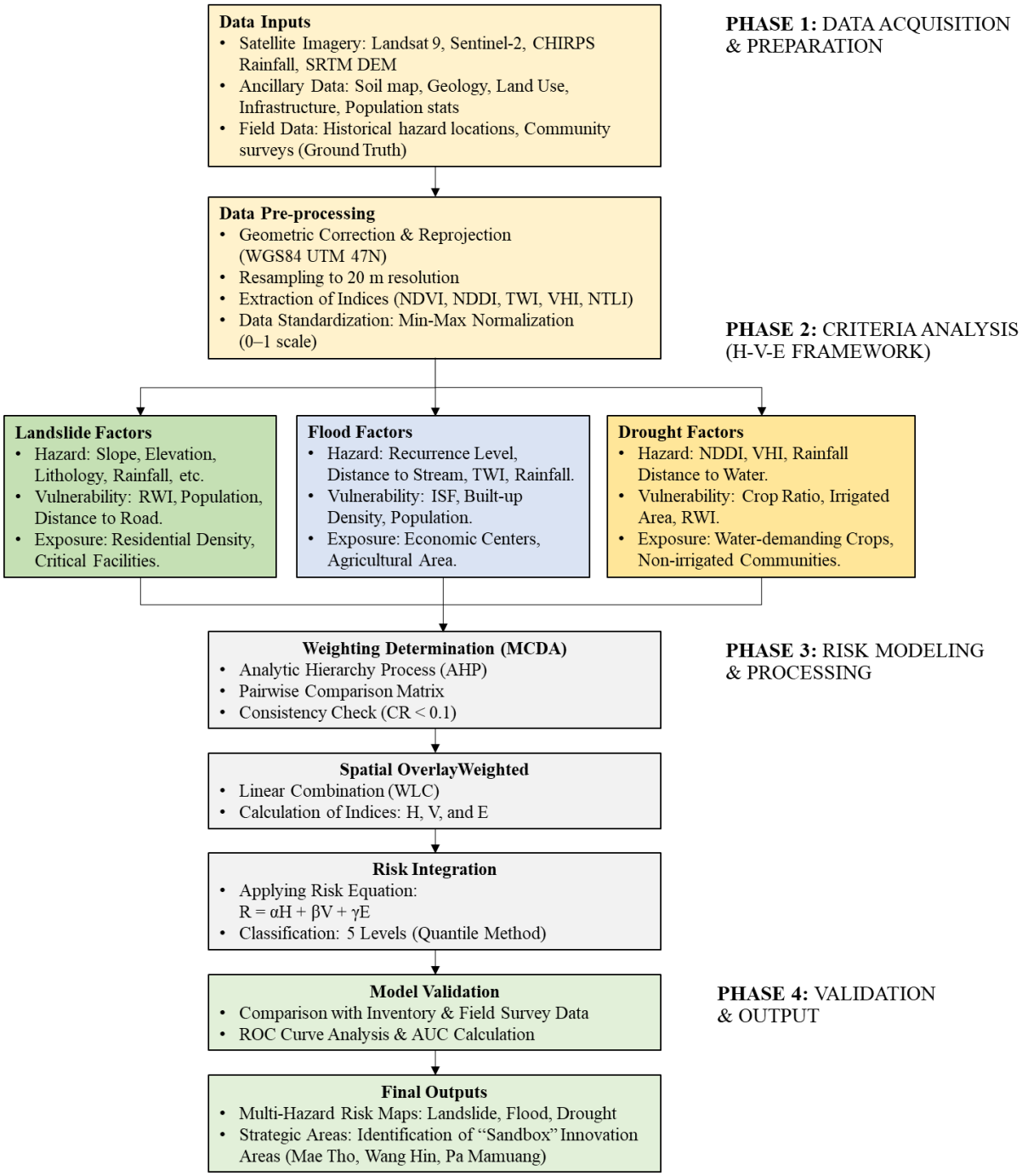

Figure 2 Methodological flowchart of multihazard risk assessment using geospatial techniques and AHP.

Table 1 Comprehensive list of data sources, temporal ranges, and spatial resolutions used in this study

Data category/factors	Data source	Period/date	Resolution/scale
Satellite imagery & climate			
Landsat 9 OLI-2/TIRS-2 (LULC, Indices)	USGS/Google Earth Engine	Feb 2025	30 m
Sentinel-2 MSI (Vegetation Indices)	ESA/Google Earth Engine	2020–2024	10 m
Precipitation (CHIRPS Daily)	UCSB/CHG	2000–2024	0.05° (~5.5 km)
Monthly average temperature	Thai Meteorological Dept. (TMD)	2000–2024	Station data
Topography (DEM & derivatives)			
Elevation, slope, TWI	USGS/NASA (SRTM DEM)	2000	30 m
Urban & built-up data			
ISF, built-up density	JRC/European Commission (GHSL)	2023	10 m
VIIRS nighttime lights	NOAA/CSM	2024	~500 m
GIS ancillary data			
Flood recurrence & extents	GISTDA	2015–2024	Vector
Administrative boundaries	Dept. of Provincial Admin. (DOPA)	2024	1:50,000
Soil texture	Land Development Dept. (LDD)	2020	1:25,000
Land use/land cover	LDD/Derived from Satellite	2024	1:25,000/10 m
Landslide points/faults/rock type	Dept. of Mineral Resources (DMR)	2020	1:50,000
Groundwater resources	Dept. of Groundwater Resources (DGR)	2023	1:50,000
Irrigation zones	Royal Irrigation Dept. (RID)	2024	1:50,000
Surface water/stream	Department of Water Resources (DWR)	2024	1:50,000
Road networks	OpenStreetMap/Ministry of Transport (MOT)	2024	1:50,000
Socioeconomic data			
Relative wealth index (RWI)	Meta (Facebook)	2021	2.4 km
Population statistics	National Statistical Office (NSO)	2024	Subdistrict level
Community field survey (Validation)	Primary Data Collection	2025	Point data (GPS)

4) Multihazard inventory and field survey

To ensure the accuracy of the risk assessment models, a comprehensive multihazard inventory was established by integrating historical datasets with primary data collected through extensive field surveys.

Historical hazard inventory: Baseline data for hazard occurrences were obtained from national agencies to serve as training and reference layers. Historical landslide occurrence points were sourced from the Department of Mineral Resources (DMR) to identify areas with a history of slope instability. For flood hazards, flood recurrence data and historical flood extents were acquired from the Geo-Informatics and Space Technology Development Agency (GISTDA). The drought-prone areas were initially identified using repeated drought reports and agricultural risk maps from local administrative organizations.

Field Surveys and Ground Truthing: A rigorous field survey was conducted to verify hazard locations and collect data on local disaster management practices. The survey employed a stratified multistage cluster random sampling method to select representative communities across the district (Cochran, 1977). A total of 462 samples were collected, which were equally distributed among the three hazard groups (154 samples each for landslides, floods, and droughts).

The survey targeted specific high-risk subdistricts identified during the preliminary analysis:

- Landslide survey focused on the Mae Tho, Nong Bua Tai, and Nong Bua Nuea subdistricts.
- Flood survey covered Tak Municipality, Nam Ruem, Mai Ngam, and Wang Hin subdistricts.

Drought survey: This study was conducted in the Wang Prachop, Pong Daeng, Taluk Klang Thung, and Pa Mamuang subdistricts.

During the fieldwork, the GPS UTM mobile application was used to record the precise geographic coordinates of past disaster events and the locations of community-based social innovations. These primary geolocated data points served as ground truth for validating the accuracy of the multihazard risk maps generated by the geospatial models.

5) Multihazard conditioning factors

The selection of conditioning factors for multihazard risk assessment was based on the hazard, vulnerability, and exposure (H-V-E) framework. A total of 42 distinct spatial factors were identified through a literature review, expert consultation (AHP panel), and

field surveys. Although some selected factors may exhibit statistical correlation, they were retained in the model because they represent distinct physical or socioeconomic mechanisms critical for disaster genesis in the local context of Mueang Tak District. For instance, while precipitation metrics are related, they function differently as either long-term climatic conditioners or immediate short-term triggers. To ensure that multicollinearity did not distort the AHP pairwise comparisons, the expert panel explicitly differentiated the functional roles of these variables during the weighting process, and a post hoc variance inflation factor (VIF) check confirmed that no variables exceeded the critical threshold of 10.

5.1) Hazard factors (H)

Hazard factors represent the physical characteristics that contribute to the occurrence or probability of a disaster. This study utilized 20 hazard conditioning factors categorized by disaster type: landslides, floods, and droughts. Key topographical and hydrometeorological indices were derived using specific equations to ensure accurate representation of physical processes (Table 2). With respect to precipitation, two distinct metrics were employed to capture different risk dimensions: annual precipitation (AP) represents long-term climatic susceptibility, whereas current year precipitation (CYP) serves as a proxy for rainfall intensity and immediate triggering events, which is consistent with standard approaches in flood and landslide modeling (Al Ali et al., 2023; Alamrew et al., 2024; Pourghasemi et al., 2012; Selvam and Jebamalai, 2023). Similarly, for drought monitoring, the NDDI was selected to specifically detect water stress in vegetation (Gu et al, 2007), complementing the VHI, which accounts for thermal stress (Kogan, 1995), thus providing a multidimensional view of agricultural drought beyond simple vegetation greenness.

To quantify hydrological and vegetative stress, spectral indices were computed using satellite imagery. The normalized difference vegetation index (NDVI) and normalized difference water index (NDWI) were first calculated to derive the normalized difference drought index (NDDI), which is effective for assessing agricultural drought severity (Gu et al, 2007). To further evaluate the combined impact of moisture deficit and thermal stress on vegetation health, the vegetation health index (VHI) was computed on the basis of the vegetation condition index (VCI) and temperature condition index (TCI) (Kogan, 1995). Additionally, the topographic wetness index (TWI) was calculated to identify areas prone to water saturation and surface runoff (Beven and Kirkby, 1979). The equations for these indices are expressed in Eqs. 1–7.

Table 2 List of conditioning factors used for hazard analysis

No.	Conditioning factors	Abbreviation	Landslide	Flood	Drought
1	Current year precipitation	CYP	✓	✓	✓
2	Annual precipitation	AP	✓	✓	✓
3	Land use and land cover	LULC	✓	✓	✓
4	Soil texture	STX	✓	✓	✓
5	Slope	SLP	✓	✓	
6	Elevation/altitude	ELV	✓	✓	
7	Landslide point density	LPD	✓		
8	Fault density	FD	✓		
9	Rock type	RT	✓		
10	Stream density	SD	✓		
11	Flood recurrence level	FRL		✓	
12	Distance from stream	DS		✓	
13	Road density	RD		✓	
14	Built-up density	BUD		✓	
15	Normalized difference drought index	NDDI			✓
16	Vegetation health index	VHI			✓
17	Distance from irrigation & wells	DIW			✓
18	Distance from surface water	DSW			✓
19	Groundwater resources	GWR			✓
20	Monthly average temperature	MAT			✓

Note: ✓ indicates that the factor was applied for that specific hazard analysis.
Distance from the stream: Natural hazard source.
Distance from Irrigation: Man-made adaptive capacity/drainage

$$\mathrm{NDVI} = (\mathrm{NIR} - \mathrm{Red})/(\mathrm{NIR} + \mathrm{Red}) \quad \text{(Eq.1)}$$

$$\mathrm{NDWI} = (\mathrm{Green} - \mathrm{NIR})/(\mathrm{Green} + \mathrm{NIR}) \quad \text{(Eq.2)}$$

$$\mathrm{NDDI} = (\mathrm{NDVI} - \mathrm{NDWI})/(\mathrm{NDVI} + \mathrm{NDWI}) \quad \text{(Eq.3)}$$

$$\mathrm{VCI} = [(\mathrm{NDVI} - \mathrm{NDVI_{min}})/(\mathrm{NDVI_{max}} + \mathrm{NDVI_{min}})] \times 100 \quad \text{(Eq.4)}$$

$$\mathrm{TCI} = [(\mathrm{LST} - \mathrm{LST_{min}})/(\mathrm{LST_{max}} - \mathrm{LST_{min}})] \times 100 \quad \text{(Eq.5)}$$

$$\mathrm{VHI} = (0.5 \times \mathrm{VCI}) + (0.5 \times \mathrm{TCI}) \quad \text{(Eq.6)}$$

$$\mathrm{TWI} = \ln(\mathrm{A}/\tan\beta) \quad \text{(Eq.7)}$$

where:

NIR, red, and green represent the spectral reflectance bands from the satellite imagery (Sentinel-2/Landsat 9).

$NDVI_{max}$ and $NDVI_{min}$ are the multiyear maximum and minimum NDVI values, respectively, for each pixel.

LST is the land surface temperature.

LST_{max} and LST_{min} are the multiyear maximum and minimum LST values, respectively, for each pixel.

A is the specific catchment area (flow accumulation).

β is the slope gradient in radians.

5.2) Vulnerability factors (V)

Vulnerability factors reflect the susceptibility of the community and physical environment to damage. This study integrated 11 factors covering social, economic, and physical dimensions (Table 3). To address the socioeconomic dimension, the RWI was employed not only as an economic indicator but also as a proxy for community coping capacity. While higher wealth can imply higher asset exposure, in the context of disaster resilience, it significantly correlates with the ability to recover and access resources (Fothergill et al., 2004). Furthermore, the ISF and distance to roads were included to reflect both physical vulnerability and the capacity for drainage and emergency accessibility, respectively.

5.3) Exposure factors (E)

Exposure refers to the presence of people, livelihoods, and assets in places that could be adversely affected. Eleven exposure factors were selected to assess the potential impact on residential areas, agriculture, and critical infrastructure (Table 4).

Table 3 List of conditioning factors used for vulnerability analysis

No.	Conditioning factors	Abbreviation	Landslide	Flood	Drought
1	Population density	PD	✓	✓	
2	Relative wealth index	RWI	✓		✓
3	Normalized difference vegetation index	NDVI	✓		✓
4	Topographic wetness index	TWI	✓		
5	Distance to roads & assistance centers	DRA	✓	✓	
6	Impervious surface fraction	ISF		✓	
7	Night-time lights intensity	NTLI		✓	
8	Building and structure proportion	BSP		✓	
9	Drought-prone crop ratio	DPCR			✓
10	Irrigated area ratio	IAR			✓
11	Agricultural area ratio	AAR			✓

Table 4 List of conditioning factors used for exposure analysis

No.	Conditioning factors	Abbreviation	Landslide	Flood	Drought
1	Residential density	RDD	✓	✓	✓
2	Critical facilities density	CFD	✓	✓	✓
3	Distance to road network	DRN	✓	✓	
4	Agricultural area density	AGD	✓	✓	✓
5	Highland villages density	HVD	✓		
6	Exposed population density	EPD	✓	✓	✓
7	Economic centers density	ECD	✓	✓	✓
8	Flood-prone settlements density	FSD	✓	✓	
9	Water-demanding crops density	WCD			✓
10	Distance to irrigation Infrastructure	DII		✓	✓
11	Nonirrigated communities density	NID			✓

6) Multihazard risk assessment models

To quantify the spatial distribution of disaster risk, an MCDA approach was employed, integrating the AHP for weight determination and the WLC for spatial overlay.

6.1) Analytic hierarchy process (AHP)

The AHP weights were derived from a panel of five experts, comprising specialists in geoinformatics and spatial risk analysis, alongside officials from the Department of Disaster Prevention and Mitigation (DDPM). This expert selection prioritizes depth of expertise and judgment consistency, aligning with established AHP methodological standards. A pairwise comparison matrix was constructed to evaluate the importance of factors within the hazard, vulnerability, and exposure domains. To ensure the logical consistency of the expert judgments, the consistency ratio (CR) was calculated. A CR value of less than or equal to 0.10 was considered acceptable. The consistency checks were performed using the following Eqs.8–10 (Saaty, 1980).

$$\lambda_{max} = 1/n \sum_{i=1}^{n} [(A \cdot w)i/wi] \quad \text{(Eq.8)}$$

$$CI = (\lambda_{max} - n)/n - 1 \quad \text{(Eq.9)}$$

$$CR = CI/RI \quad \text{(Eq.10)}$$

where:

λmax is the principal eigenvalue of the matrix.
n is the number of factors.
CI is the consistency index.
RI is the random index dependent on n.
w is the weight vector.

6.2) Determination of risk factors and weights

The AHP was applied to prioritize conditioning factors, with all CRs calculated below 0.10, ensuring the reliability of expert judgments.

- **Landslide risk weights**

With respect to landslide hazard, slope (SLP) was the most significant factor (w=0.2782), followed by landslide point density (w=0.2064) and fault density (w=0.1523) (Table 5). This weighting aligns with geomorphological principles where steep terrain dictates mass movements. With respect to vulnerability, the relative wealth index (RWI) held the highest weight (w=0.5954), suggesting that economic capacity is crucial for coping. With respect to exposure, residential density (RDD) was the dominant factor (w=0.3268), highlighting the risk to settlements in slope-prone areas.

Table 5 Weights of conditioning factors for landslide risk assessment

Component	Conditioning factors	Abbreviation	Weight (wi)
Hazard	Slope	SLP	0.2782
	Landslide point density	LPD	0.2064
	Fault density	FD	0.1523
	Rock type	RT	0.1094
	Soil texture	STX	0.0804
	Current year precipitation	CYP	0.0680
	Stream density	SD	0.0415
	Land use and land cover	LULC	0.0279
	Annual precipitation	AP	0.0205
	Elevation/altitude	ELV	0.0154
Vulnerability	Relative wealth index	RWI	0.5954
	Normalized difference vegetation index	NDVI	0.1709
	Distance to roads & assistance centers	DRA	0.1276
	Topographic wetness index	TWI	0.0579
	Population density	PD	0.0482
Exposure	Residential density	RDD	0.3268
	Critical facilities density	CFD	0.2273
	Highland villages density	HVD	0.1569
	Distance to road network	DRN	0.1077
	Agricultural area density	AGD	0.0734
	Exposed population density	EPD	0.0497
	Economic centers density	ECD	0.0341
	Flood-prone settlements density	FSD	0.0241

- **Flood risk weights**

In the flood hazard analysis, the flood recurrence level (FRL) was the most influential factor (w=0.2928), followed by slope (w=0.1699) and annual precipitation (w=0.1466) (Table 6). With respect to vulnerability, the ISF received the highest weight (w=0.4190), indicating that urbanization and surface sealing significantly exacerbate flood impacts. Like landslides, residential density (w=0.3196) remained the primary exposure factor.

- **Drought risk weights**

With respect to drought hazard, the NDDI and VHI were deemed equally important (w=0.2337), reflecting their efficacy in monitoring vegetation stress (Table 7). Vulnerability was driven primarily by the drought-prone crop ratio (w=0.3738), highlighting the sensitivity of specific agricultural practices. With respect to exposure, residential density (w=0.3171) and critical facility density (w=0.2197) were the leading factors.

Table 6 Weights of conditioning factors for flood risk assessment

Component	Conditioning factors	Abbreviation	Weight (wi)
Hazard	Flood recurrence level	FRL	0.2928
	Slope	SLP	0.1699
	Annual precipitation	AP	0.1466
	Current Year precipitation	CYP	0.1426
	Distance from stream	DS	0.0977
	Road density	RD	0.0513
	Built-up density	BUD	0.0379
	Elevation/altitude	ELV	0.0233
	Soil texture	STX	0.0199
	Land use and land cover	LULC	0.0180
Vulnerability	Impervious surface fraction	ISF	0.4190
	Population density	PD	0.2485
	Night-time lights intensity	NTLI	0.1518
	Building and structure proportion	BSP	0.1151
	Distance to roads & assistance centers	DRA	0.0656
Exposure	Residential density	RDD	0.3196
	Critical facilities density	CFD	0.2234
	Economic centers density	ECD	0.1493
	Distance to road network	DRN	0.1162
	Agricultural area density	AGD	0.0788
	Exposed population density	EPD	0.0486
	Flood-prone dettlements density	FSD	0.0351
	Distance to irrigation infrastructure	DII	0.0290

- **Data standardization and weighted linear combination (WLC)**

Before the weights were applied, all the conditioning factors were standardized to a uniform scale of 0 to 1 to ensure comparability. Prior to normalization, the categorical datasets (e.g., soil texture and rock type) were converted into numerical values using a susceptibility scoring approach, where higher scores were assigned to classes with greater inherent instability or sensitivity on the basis of the literature and historical occurrence ratios. The min–max normalization method was applied on the basis of the relationship between each factor and the risk occurrence (Table 8).

For factors with a positive relationship (where higher values increase risk, e.g., slope), Eq.11 was used. Conversely, for factors with a negative relationship (where higher values decrease risk, e.g., distance from the stream), Eq.12 was applied (Jiang and Eastman, 2000; Malczewski, 1999) .

$$\mu(x) = (x_i - x_{min})/(x_{max} - x_{min})$$ (Positive relationship) (Eq.11)

$$\mu(x) = (x_{max} - x_i)/(x_{max} - x_{min})$$ (Negative relationship) (Eq.12)

where:

$\mu(x)$ is the standardized score (0–1).

X_i is the raw value of the factor.

X_{min} and X_{max} are the minimum and maximum values observed in the study area, as detailed in Table 8.

Table 7 Weights of conditioning factors for drought risk assessment

Component	Conditioning factors	Abbreviation	Weight (wi)
Hazard	Normalized difference drought index	NDDI	0.2337
	Vegetation health index	VHI	0.2337
	Annual precipitation	AP	0.1998
	Current year precipitation	CYP	0.1096
	Distance from irrigation & wells	DIW	0.0633
	Distance from surface water	DSW	0.0427
	Groundwater resources	GWR	0.0366
	Land use and land cover	LULC	0.0361
	Soil texture	STX	0.0234
	Monthly average temperature	MAT	0.0212
Vulnerability	Drought-prone crop ratio	DPCR	0.3738
	Irrigated area ratio	IAR	0.2764
	Agricultural area ratio	AAR	0.1742
	Normalized difference vegetation index	NDVI	0.1024
	Relative wealth index	RWI	0.0732
Exposure	Residential density	RDD	0.3171
	Critical facilities density	CFD	0.2197
	Water-demanding crops density	WCD	0.1579
	Agricultural area density	AGD	0.1180
	Distance to irrigation infrastructure	DII	0.0798
	Exposed population density	EPD	0.0484
	Nonirrigated communities density	NID	0.0341
	Economic centers density	ECD	0.0250

Table 8 Statistical characteristics and standardization direction of the conditioning factors

Conditioning factors	Abbreviation	Unit	Min	Max	Relationship to risk*
Topographical					
Elevation/altitude	ELV	m	91.00	1,190.00	Positive/negative**
Slope	SLP	Degree	0.00	72.59	Positive/negative**
Hydrometeorological					
Annual precipitation	AP	mm	1,298.00	1,352.00	Positive (LS, FL)/negative (DR)
Current year precipitation	CYP	mm	1,185.00	1,240.00	Positive (LS, FL)/negative (DR)
Monthly Average temperature	MAT	°C	19.16	24.02	Positive
Normalized difference drought index	NDDI	Index	0.11	0.86	Positive
Vegetation health index	VHI	Index	0.19	0.80	Negative
Hydrological					
Flood recurrence level	FRL	Times	0.00	5.00	Positive
Distance from stream	DS	km	0.00	27.28	Negative
Distance from irrigation & wells	DIW	km	0.00	21.91	Positive
Distance from surface water	DSW	km	0.00	21.45	Positive
Stream density	SD	Classes	0.00	5.00	Positive
Anthropogenic & others					
Road density	RD	Classes	0.00	5.00	Positive
Built-up density	BUD	Classes	0.00	5.00	Positive
Landslide point density	LPD	Classes	0.00	5.00	Positive
Fault density	FD	Classes	0.00	5.00	Positive
Categorical factors (Scored)					
Land use and land cover	LULC	Score	0.00	1.00	Positive
Soil texture	STX	Score	0.00	1.00	Positive
Rock type	RT	Score	0.00	1.00	Positive
Groundwater resources	GWR	Score	0.00	1.00	Positive

Note: Relationship to Risk:
Positive: A higher value indicates a greater risk (e.g., higher slope = higher landslide risk).
Negative: A higher value decreases risk (e.g., a higher VHI = lower drought risk).
Depending on Hazard: Some factors act differently depending on the disaster type (e.g., high elevation increases landslide risk but decreases flood risk).
Scored: These factors were qualitative data converted into a quantitative score (0-1) on the basis of their degree of susceptibility.

- **Weighted linear combination (WLC)**

Following the weight calculation, the WLC method was applied to aggregate the normalized factor layers. This process involved multiplying each standardized factor (X_i) by its corresponding weight (w_i) and summing the results to generate the composite indices for hazard (H), vulnerability (V), and exposure (E). The general aggregation equation is expressed as Eq.13 (Jiang and Eastman, 2000; Malczewski, 1999; 2000).

$$S = \sum_{i=1}^{n} w_i x_i \quad \text{(Eq.13)}$$

where S represents the composite index score (e.g., hazard index), and $\sum_{i=1}^{n} w_1 = 1$

- **Risk model integration**

The final multihazard risk index (R) was modeled as a linear function of the three aggregated components. Unlike multiplicative risk models, this study adopted a weighted summation approach to explicitly account for the additive contribution of each component to the total risk, defined as Eq.14.

$$R = \alpha H + \beta V + \gamma E \quad \text{(Eq.14)}$$

where:

H, V, and E are the calculated indices for hazard, vulnerability, and exposure, respectively.

α, β, and γ are the weights assigned to each component.

In this study, equal weights were applied (α = β = γ = 1.0), assuming that all three dimensions contributed equally to the overall disaster risk magnitude. This unweighted summation avoids introducing subjective bias at the integration stage, ensuring that the final risk distribution reflects the composite interaction of the AHP-weighted subfactors (Al Ali et al., 2023; Malczewski, 2000).

The resulting risk values were subsequently reclassified into five qualitative levels—very low, low, moderate, high, and very high—using the quantile classification method. This method was selected to distribute the spatial values equally across classes, ensuring that the highest risk categories clearly highlight the top tier of at-risk areas relative to the entire district. This interpretation emphasizes relative prioritization for resource allocation, preventing the suppression of high-risk clusters that might occur with absolute threshold methods.

7) Model validation

To evaluate the reliability and predictive accuracy of the generated risk maps, the receiver operating characteristic (ROC) curve method was employed. This technique validates the spatial models by comparing the probabilistic risk values against independent ground-truth data. The validation dataset included 462 verified hazard locations (154 points per hazard type) obtained exclusively from the field surveys described in the previous section. To address potential spatial dependence and bias, these samples were collected using a stratified multistage cluster random sampling method, ensuring a spatially balanced distribution across diverse topographical and administrative zones (Cochran, 1977).

The validation process involved plotting the true positive rate (sensitivity) against the false positive rate (1 - specificity) across various threshold settings. The area under the curve (AUC) was then calculated to quantify the model's performance. The AUC value ranges from 0.5 to 1.0, where values closer to 1.0 indicate higher accuracy. In this study, the performance was categorized as follows: 0.5–0.6 (poor), 0.6–0.7 (average), 0.7–0.8 (good), 0.8–0.9 (very good), and 0.9–1.0 (excellent). Separate validation procedures were conducted for the landslide, flood, and drought risk models to ensure the robustness of each specific hazard assessment (Hosmer et al., 2013; Yesilnacar et al., 2005).

Results

1) Spatial distribution of multihazard risks

The integration of the hazard, vulnerability, and exposure indices (R = αH + βV + γE) generated spatially explicit risk maps classified into five levels: very low to very high.

1.1) Landslide risk distribution

The spatial distributions of landslide components—hazard, vulnerability, and exposure—are illustrated in Figure 3. The final risk map (Figure 4) reveals that high-risk zones are predominantly concentrated in the rugged western highlands and are directly correlated with physical geography where slope gradients frequently exceed 45 degrees. The Mae Tho Subdistrict was identified as the most critical area, where the hazard is driven by steep terrain and weathered lithology. Statistical analysis revealed that high- and very high-risk zones cover approximately 9.97% and 1.88% of the district, respectively. In contrast, the eastern flatlands (e.g., Wang Hin and Taluk Klang Thung) exhibited minimal risk because of their low-lying topography, with 80.52% classified as low- to no-risk areas.

1.2) Flood risk distribution

The flood hazard, vulnerability, and exposure maps are presented in Figure 5. The integrated flood risk assessment (Figure 6) revealed spatially clustered risk zones along the Ping River floodplain, which acted as the district's main hydrological artery. Tak Municipality and adjacent subdistricts such as Pa Mamuang were identified as the most susceptible areas. The high risk in these urban zones is driven by the convergence

of low elevation and high exposure (dense settlements), whereas the extensive ISF amplifies vulnerability by reducing natural infiltration. The quantitative results reveal that approximately 8.09% and 0.68% of the districts fall under the high- and very high-risk categories, respectively. Conversely, the western upland areas remain largely unaffected (82.13% Very Low-non risk).

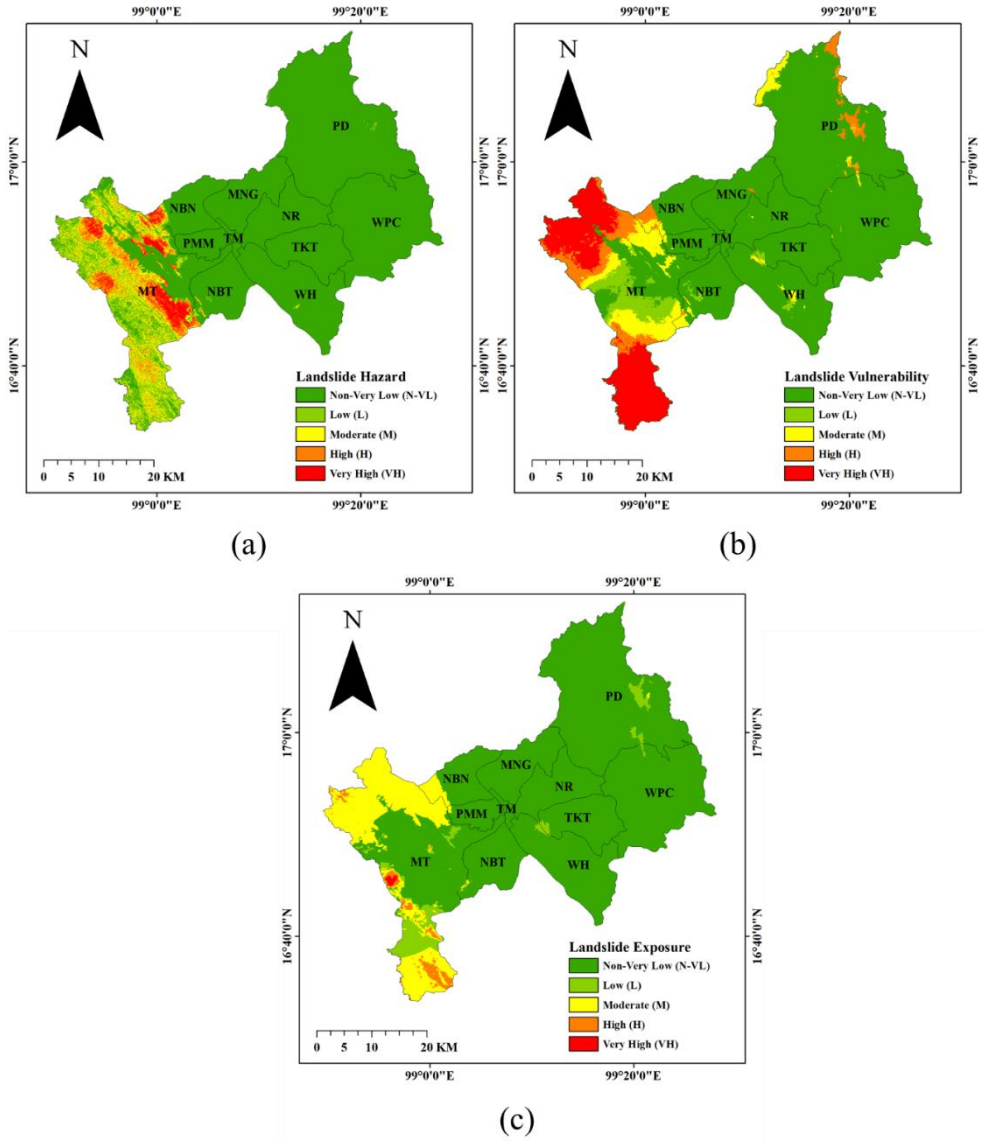

Figure 3 Spatial distribution of landslide (a) hazard (b) vulnerability and (c) exposure in Mueang Tak District.

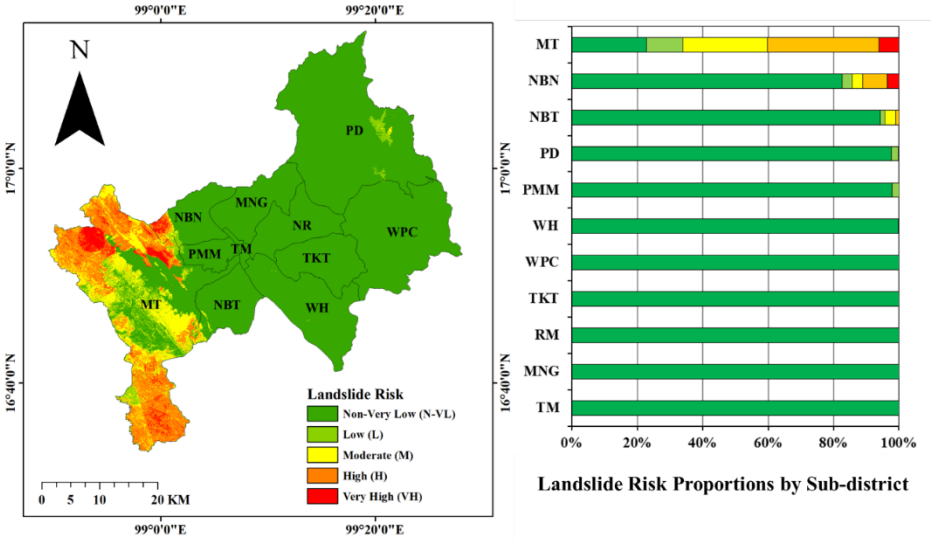

Figure 4 Spatial distribution of landslide risk in Mueang Tak District.

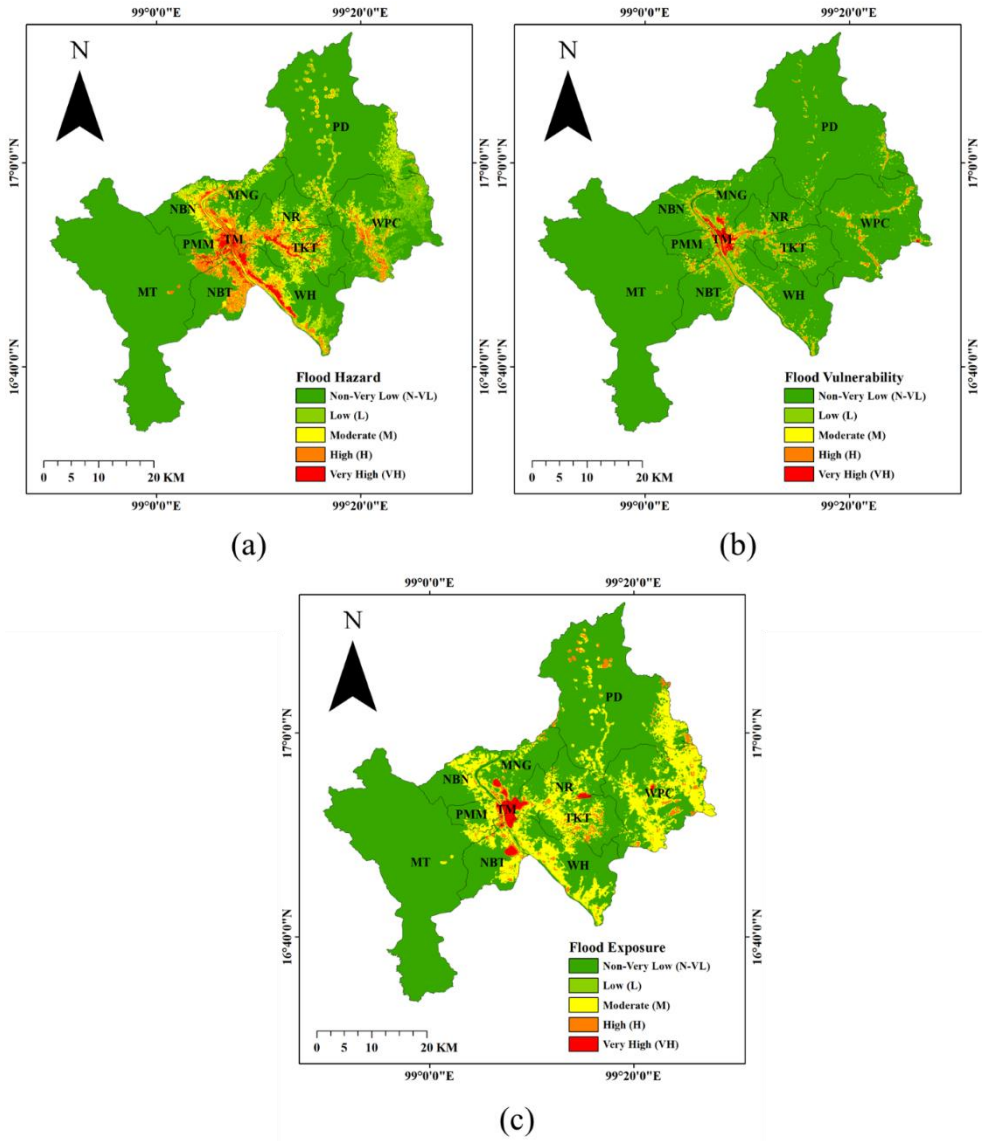

Figure 5 Spatial distribution of flood (a) hazard (b) vulnerability and (c) exposure in Mueang Tak District.

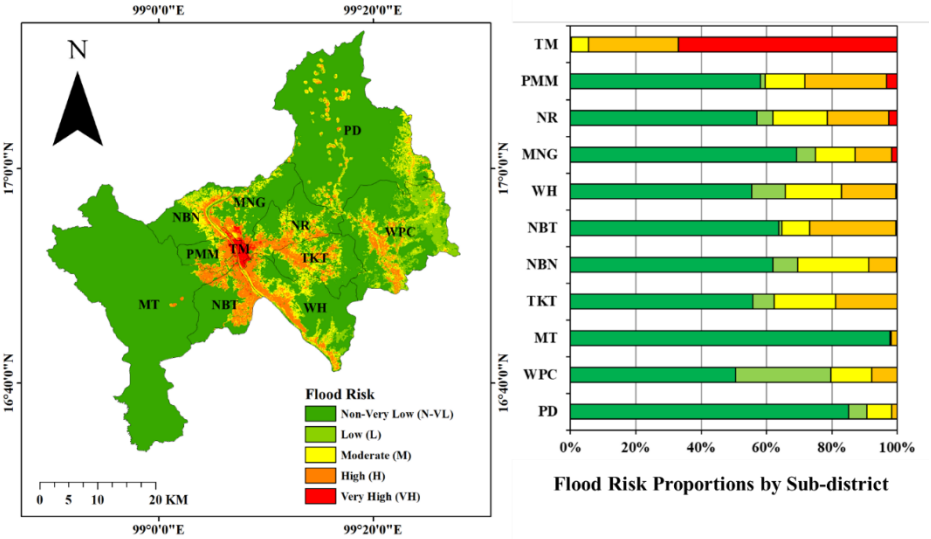

Figure 6 Spatial distribution of flood risk in Mueang Tak District.

1.3) Drought risk distribution

The spatial patterns of drought hazard, vulnerability, and exposure are depicted in Figure 7. The resulting drought risk map (Figure 8) exhibits a contrasting pattern, which is most pronounced in the eastern rain-fed agricultural belts outside the irrigation network. Pa Mamuang, Wang Prachop and Taluk Klang Thung were classified as the most vulnerable because of their reliance on water-intensive monoculture crops (e.g., cassava and rice) without access to the Ping River system. Consequently, drought risk has the most extensive spatial coverage, with high- and very high-risk zones encompassing a significant portion of the district (14.96% and 2.86%, respectively). This extensive spread highlights the urgent need for decentralized water management interventions in these agricultural zones.

1.4) Comparative area analysis

The area analysis reveals that drought risk has the most extensive spatial coverage. In comparison, flood risk is more localized but highly intensive in urban centers, whereas landslide risk is confined to specific geomorphological zones in the west.

2) Model validation

The ROC curve and AUC were employed to validate the AHP-based models against ground-truth data (Figure 9).

2.1) Landslide risk model validation

The landslide model yielded an AUC value of 0.867, indicating very good predictive ability. These findings confirm that slope and land cover factors effectively delineate landslide-prone areas in mountainous regions.

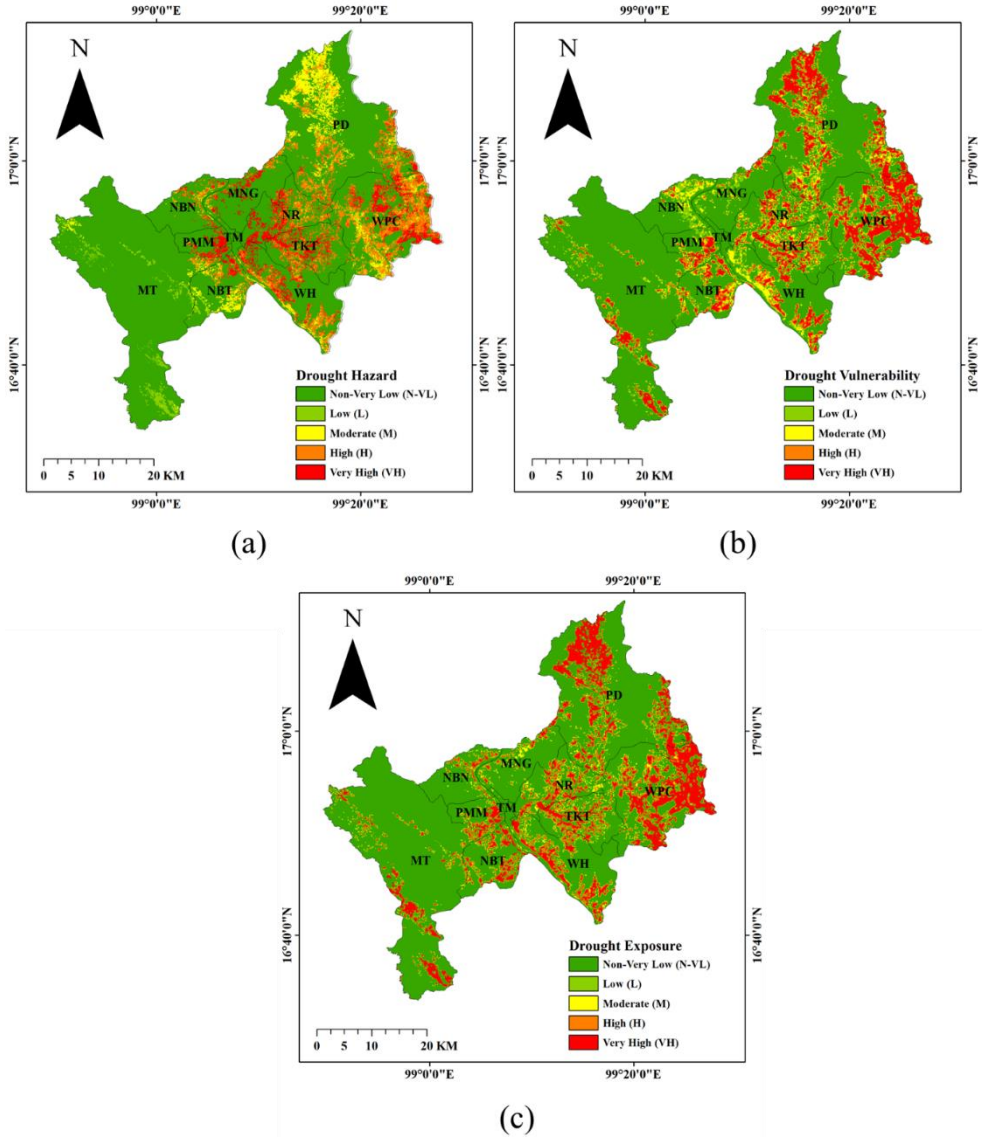

Figure 7 Spatial distribution of drought (a), hazard (b), and vulnerability and (c) exposure in Mueang Tak District.

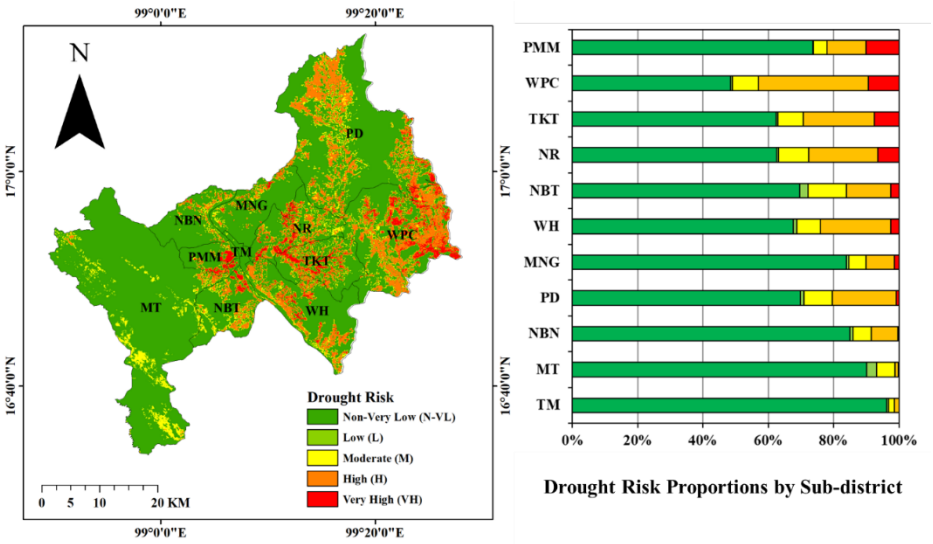

Figure 8 Spatial distribution of drought risk in Mueang Tak District.

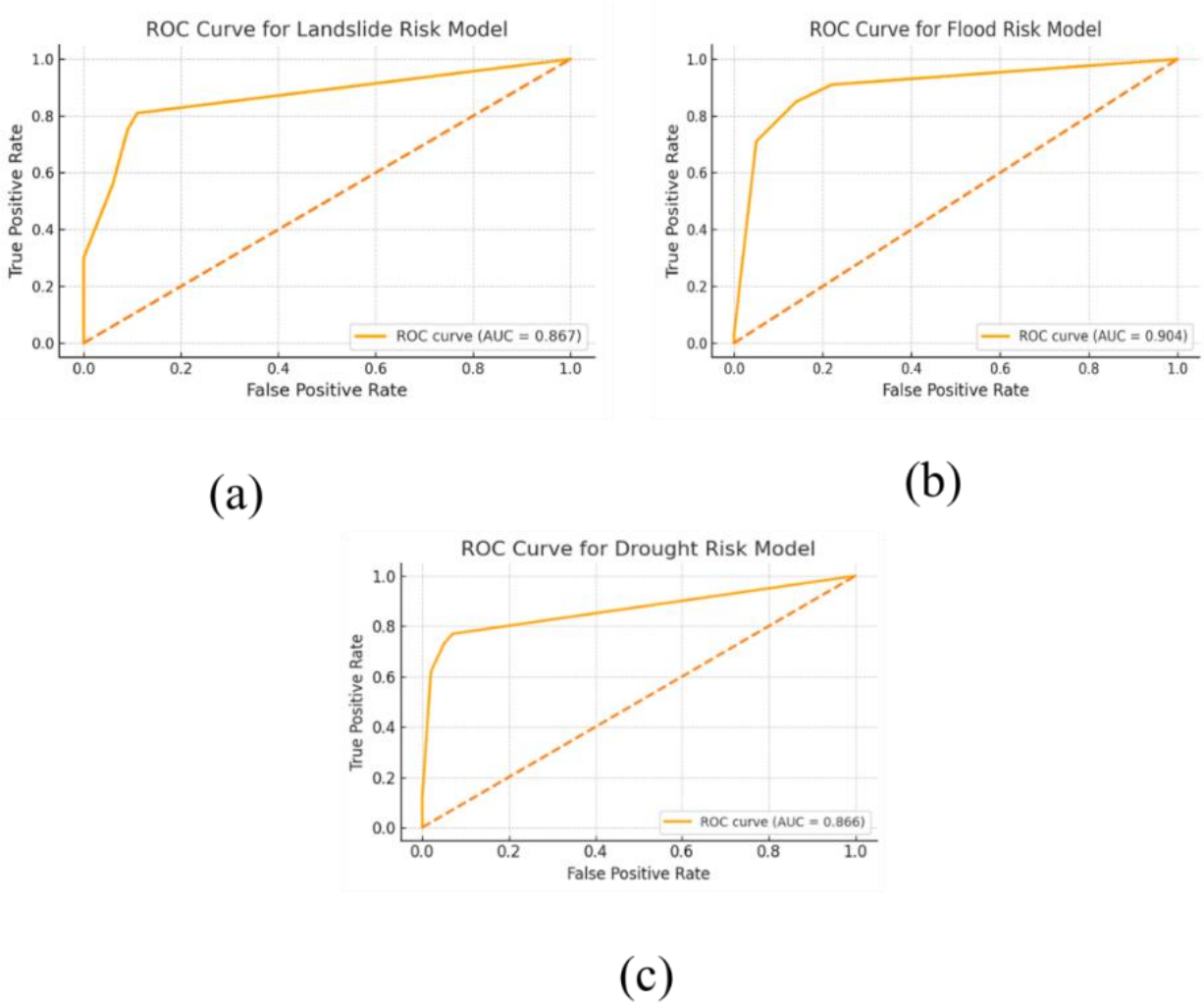

Figure 9 ROC curve and AUC values for the risk assessment model (a) landslides (b) floods and (c) drought.

2.2) Flood risk model validation

The flood risk model achieved an AUC of 0.904, indicating an excellent level of accuracy. The model successfully identified critical flood zones along the Ping River Basin, validating the high weights assigned to recurrence levels and impervious surfaces.

2.3) Validation of the drought risk model

The drought model demonstrated very good performance, with an AUC of 0.866. This substantiates the use of satellite-derived indices (NDDI and VHI) for monitoring agricultural drought in nonirrigated zones.

2.4) Overall model performance

Overall, all three hazard models exhibited AUC values exceeding 0.85, confirming their robustness for spatial planning and supporting the development of the disaster risk reduction sandbox.

Discussion

1) Methodological effectiveness

The multihazard risk assessment in this study demonstrates the robustness of integrating the H-V-E framework with the AHP. The validation results yielded satisfactory AUC values, confirming that expert-driven knowledge (AHP) remains a reliable approach for spatial modeling, particularly when complex socioeconomic variables that quantitative data-driven models might overlook are integrated. These findings complement those of Aldiansyah et al. (2025), who compared statistical models (Dempster–Shafer; DS, statistical index; SI, and certainty factor; CF) for landslide mapping in Indonesia. While Aldiansyah et al. (2025) reported that data-driven models such as CF provided high accuracy (AUC = 81.02%) based purely on physical conditioning factors, our study suggests that the AHP offers a distinct advantage in multihazard contexts by allowing the flexible incorporation of "vulnerability" and "exposure" weights, which are critical for policy planning in semiurban districts such as Mueang Tak. Furthermore, our results support Hussain et al. (2021), who noted that the AHP is particularly effective for local-scale management where transparency in decision criteria is required for stakeholder communication.

2) Hazard-specific insights

Landslides: The identification of slope (w=0.2782) as the primary landslide driver aligns with global geomorphological studies. The high-risk concentration in the steep terrain of Mae Tho Subdistrict corroborates the findings of Abay et al. (2025), who reported that slope gradient and land cover degradation are the dominant predictors of instability in mountainous regions.

Floods: In terms of flood risk, the strong influence of the ISF (w=0.4190) in Tak Municipality highlights the anthropogenic impact on hydrological dynamics. This finding is consistent with those of Chomani (2024) and Waseem et al. (2023), who emphasized that urban expansion and surface sealing significantly amplify flood susceptibility by disrupting natural drainage systems in river basins.

Droughts: This study uniquely reveals that drought risk in Mueang Tak is driven not only by meteorological deficiency but also by structural vulnerability (e.g., lack of irrigation). This finding validates the multidimensional approach proposed by Tela et al. (2024), who argued that integrating socioeconomic coping capacities with physical indices (such as the NDDI) provides a more realistic depiction of agricultural drought risk than using rainfall data alone does.

3) Practical implications for disaster sandboxes

Beyond theoretical modeling, this research translates spatial risk findings into actionable policy measures for the "disaster risk reduction sandbox" initiative. By pinpointing specific high-risk clusters, local authorities can transition from blanket policies to targeted interventions suited to the potential and limitations of each community:

Landslide management (Target: Mae Tho Subdistrict): Given the steep terrain and limited infrastructure in Mae Tho, short-term measures should prioritize "knowledge-based surveillance", such as training local volunteers to monitor simple rain gauges and recognize early signs of slope failure. Long-term projects should focus on low-cost bioengineering, specifically promoting the planting of deep-rooted vegetation (e.g., vetiver grass) on critical slopes to enhance soil stability without the need for heavy construction machinery.

Flood management (Target: Wang Hin Subdistrict): The risk in urban zones is driven by impervious surfaces. Short-term actions must focus on the pre-monsoon dredging of drainage networks identified in high-exposure map layers. For long-term resilience, urban planning policies should integrate "green Infrastructure" concepts, such as enforcing permeable pavement regulations in new development areas and expanding retention areas (Kaem Ling) to buffer excess runoff.

Drought management (Target: Pa Mamuang Subdistrict): In these rain-fed agricultural belts, risk reduction relies on adaptation. Short-term strategies involve disseminating seasonal climate forecasts to help farmers adjust their crop calendars. Long-term investments should support community-scale water innovations, such as groundwater banking or small-scale reservoirs, to reduce dependency on erratic rainfall.

By adopting these evidence-based measures, "sandbox" areas can demonstrate how local administrative organizations (LAOs) can effectively utilize spatial data to minimize impacts and enhance community safety.

Conclusions

This study successfully established a comprehensive multihazard risk assessment for Mueang Tak District by integrating the H-V-E framework with geospatial techniques and the AHP. The results provide a spatially explicit understanding of disaster risk, revealing distinct geographical patterns driven by diverse topographical and socioeconomic contexts.

The analysis revealed that landslide risk is concentrated in steep, mountainous western regions, particularly in Mae Tho Subdistrict, and is driven primarily by slope

gradient and lithology. Flood risks are intensified in the urbanized lowlands along the Ping River, specifically in Tak Municipality, where high impervious surface fractions exacerbate drainage issues. Conversely, drought risks dominate the eastern rain-fed agricultural belts, such as the Wang Prachop and Pa Mamuang Subdistricts, largely because of the dependency on monoculture crops and limited irrigation infrastructure.

Methodological validation confirmed the robustness of the AHP-based geospatial model, yielding high prediction accuracies, with AUC values of 0.867 for landslides, 0.904 for floods, and 0.866 for droughts. These findings underscore that integrating expert-driven weighting with quantitative spatial data significantly enhances the reliability of local-scale risk modeling.

From a policy perspective, this research offers a scientific foundation for the operationalization of the “disaster risk reduction sandbox”. By delineating high-risk zones with precision, local authorities can prioritize resource allocation and implement targeted interventions —such as reforestation in landslide-prone areas, drainage upgrades in urban flood zones, and the development of community water reservoirs in drought-stricken localities. Ultimately, this study advocates for a shift from reactive disaster relief to proactive, data-driven community-based disaster risk management (CBDRM), fostering long-term resilience for the communities of Mueang Tak District (Räsänen et al., 2020; Van Niekerk et al., 2017,).

Limitations and future work

Despite the high predictive accuracy achieved, this study has certain limitations. First, the final risk maps were derived by resampling multisource geospatial data with varying original spatial resolutions—ranging from high-resolution satellite imagery to coarser climatic and socioeconomic datasets—in a unified 20-meter grid. This process, while necessary for spatial integration, may introduce inherent uncertainties related to downscaling and the interpolation of lower-resolution inputs. Second, while the AHP provides a robust framework for integrating socioeconomic variables, the weighting process inherently relies on expert judgment, which may introduce subjective bias. Finally, the current model focuses on static risk factors; therefore, future research should incorporate real-time hydro-meteorological data and machine learning algorithms to increase the precision of dynamic predictions and account for the evolving impacts of climate change.

Acknowledgements

This research was supported by the Science Research and Innovation Promotion Fund, Fundamental Fund (FF) for the fiscal year 2025. The authors would like to express their gratitude to Kamphaeng Phet Rajabhat University for providing the necessary facilities and to the local administrative organizations in Mueang Tak District for their cooperation during the field surveys and data collection process.

Data availability statement

Information and data used in the study will be disclosed upon request.

Author ORCID

Suphatphong Ruthamnong:

Author contributions

Suphatphong Ruthamnong:

Limitations and future work

Conflicts of interest

The authors declare that there are no conflicts of interest in competing financial or personal relationships that could have appeared to influence the work reported in this work.

References

Abay, A., Mulugeta, A., & Mebrahtu, G. (2025). GIS-based landslide susceptibility mapping using frequency ratio method: A case study from Adigrat-Mugulat mountain chains, northern Ethiopia. *Scientific African*, *28*, e02661.

Al Ali, A. M., Salih, A., & Hassaballa, A. (2023). Geospatial-based analytical hierarchy process (AHP) and weighted product model (WPM) techniques for mapping and assessing flood susceptibility in the Wadi Hanifah drainage basin, Riyadh region, Saudi Arabia. *Water*, *15*(10), 1943.

Alamrew, B. T., Kassawmar, T., Mengstie, L., & Jothimani, M. (2024). Combined GIS, FR and AHP approaches to landslide susceptibility and risk zonation in the Baso Liben district, Northwestern Ethiopia. *Quaternary Science Advances*, *16*, 100250.

Aldiansyah, S., Ati, A., & Saudi, F. (2025). Landslide susceptibility mapping via Dempster-Shafer, statistical index, and certainty factor models in GIS and their comparison at Pidie Regency in Aceh, Indonesia. *Applied Environmental Research*, *47*(4), 1–22.

Alharbi, R. S., Nath, S., Faizan, O. M., Hasan, M. S. U., Alam, S., Khan, M. A.,Bakshi, S., Sahana, M., & Saif, M. M. (2022). Assessment of drought vulnerability through an integrated approach using AHP and geoinformatics in the Kangsabati River Basin. *Journal of King Saud University - Science*, *34*(8), 102332.

de Azevedo Reis, G., de Souza Filho, F. A., Nelson, D. R., Rocha, R. V., & da Silva, S. M. O. (2020). Development of a drought vulnerability index using MCDM and GIS: Study case in São Paulo and Ceará, Brazil. *Natural Hazards*, *104*, 1781–1799.

Beven, K. J., & Kirkby, M. J. (1979). A physically based, variable contributing area model of basin hydrology. *Hydrological Sciences Bulletin*, *24*(1), 43–69.

Chi, G., Fang, H., Chatterjee, S., & Blumenstock, J. E. (2022). Microestimates of wealth for all low-and middle-income countries. *Proceedings of the National Academy of Sciences*, *119*(3), e2113658119.

Chomani, K. (2024). Assessing the impact of urbanization on flood hazards in Ranya City, using GIS and remote sensing. *Eurasian Journal of Science and Engineering*, *9*, 154–165.

Cochran, W. G. (1977). *Sampling techniques* (3rd ed.). John Wiley & Sons.

Department of Provincial Administration (DOPA). (2024). *General information of Mueang Tak District*. Ministry of Interior. https://www.dopa.go.th

Elvidge, C. D., Baugh, K., Zhizhin, M., Hsu, F. C., & Ghosh, T. (2017). VIIRS night-time lights. *International Journal of Remote Sensing*, *38*(21), 5860–5879.

Fothergill, A., & Peek, L. A. (2004). Poverty and disasters in the United States: A review of recent sociological findings. *Natural Hazards*, *32*(1), 89–110.

Funk, C., Peterson, P., Landsfeld, M., Pedreros, D., Verdin, J., Shukla, S., Husak, G., Rowland, J., Harrison, L., Hoell, A., & Michaelsen, J. (2015). The climate hazards infrared precipitation with stations—A new environmental record for monitoring extremes. *Scientific Data*, *2*(1), 1–21, 2015.

Gorelick, N., Hancher, M., Dixon, M., Ilyushchenko, S., Thau, D., & Moore, R. (2017). Google Earth Engine: Planetary-scale geospatial analysis for everyone. Remote Sensing of Environment, 202, 18–27.

Gu, Y., Brown, J. F., Verdin, J. P., & Wardlow, B. D. (2007). A five-year analysis of MODIS NDVI and NDWI for grassland drought assessment over the central Great Plains of the United States. *Geophysical Research Letters*, *34*(6), L06407.

Hosmer, D. W., Lemeshow, S., & Sturdivant, R. X. (2013). *Applied logistic regression* (3rd ed.). John Wiley & Sons.

Hussain, M., Tayyab, M., Zhang, J., Shah, A. A., Ullah, K., Mehmood, U., & Al-Shaibah, B. (2021). GIS-based multi-criteria approach for flood vulnerability assessment and mapping in District Shangla: Khyber Pakhtunkhwa, Pakistan. *Sustainability*, *13*(6), 3126.

IPCC. (2012). *Managing the risks of extreme events and disasters to advance climate change adaptation: A special report of the Intergovernmental Panel on Climate Change*. Cambridge University Press.

Jiang, H., & Eastman, J. R. (2000). Application of fuzzy measures in multi-criteria evaluation in GIS. *International Journal of Geographical Information Science*, *14*(2), 173–184.

Kamphaeng Phet Rajabhat University. (2018). *History of Mueang Tak District and important natural resources*. Academic Resources and Information Technology Center. https://arit.kpru.ac.th/ap/local/?nu=pages&page_id=658

Kayastha, P., Dhital, M. R., & De Smedt, F. (2013). Application of the analytical hierarchy process (AHP) for landslide susceptibility mapping: A case study from the Tinau watershed, west Nepal. *Computers & Geosciences*, *52*, 398–408.

Kogan, F. N. (1995). Application of vegetation index and brightness temperature for drought detection. *Advances in Space Research*, *15*(11), 91–100.

Kukuntod, N., & Wijitkosum, S. (1999). Drought vulnerability assessment in Lam Ta Kong Watershed. In Pal, I., Mukhopadhyay, A., Virdis, S.G., & Tawhidul Islam, S. (Eds.), *Proceedings of the 3rd International Symposium on Disaster Resilience and Sustainable Development—Volume 3* (pp. 13–24). Springer.

Malczewski, J. (1999). *GIS and multicriteria decision analysis*. John Wiley & Sons.

Malczewski, J. (2000). On the use of weighted linear combination method in GIS: Common and best practice approaches. *Transactions in GIS*, *4*(4), 249–268.

Muhimbula, J., Sumari, N. S., Balz, T. (2025). Landslide susceptibility assessment using AHP, frequency ratio, and LSI models: Understanding topographical controls in Hanang District, Tanzania. *GeoHazards*, *6*(3), 58.

Mulabbi, A., Esagu, J. C., Akello, G., & Turyahabwe, R. (2025). Assessment of landslide susceptibility and settlement exposure via geospatial techniques in Bulambuli District, Eastern Uganda. *Applied Environmental Research*, *47*(4), 1–17.

Office of the Permanent Secretary, Ministry of Agriculture and Cooperatives. (2025). *General information of Tak Province: Climate and seasons*. https://www.opsmoac.go.th/tak-dwl-files-471391791079

Pesaresi, M., Huadong, G., Blaes, X., Ehrlich, D., Ferri, S., Gueguen, L., Halkia, M., Kauffmann, M., Kemper, T., Lu, L., Marin-Herrera, M. A., Ouzounis, G. K., Scavazzon, M., Soille, P., Syrris, V., & Zanchetta, L. (2013). A global human settlement layer from optical HR/VHR RS data: Concept and first results. *IEEE Journal of Selected Topics in Applied Earth Observations and Remote Sensing*, *6*(5), 2102–2131.

Pourghasemi, H. R., Pradhan, B., & Sezer, E. A. (2012). Landslide susceptibility mapping using application of fuzzy logic and analytical hierarchy process (AHP) at Haraz Watershed, Iran. *Geomatics, Natural Hazards and Risk*, *3*(2), 111–143.

Räsänen, A., Lein, H., Bird, D., & Setten, G. (2020). Conceptualizing community in disaster risk management. *International Journal of Disaster Risk Reduction*, *45*, 101485.

Ruthamnong, S., Wattanatasanee, B., & Klomklamnum, I. (2023). *Geoinformatics innovation for creating spatial knowledge to reduce threats to quality of life towards enhancing community-based risk management capabilities in Mae Sot District, Tak Province*. National Research Council of Thailand.

Saaty, T. L. (1980). *The analytic hierarchy process: Planning, priority setting, resource allocation*. McGraw-Hill.

Selvam, R. A., & Jebamalai, A. R. A. (2023). Application of the analytical hierarchy process (AHP) for flood susceptibility mapping using GIS techniques in Thamirabarani river basin, Srivaikundam region, Southern India. *Natural Hazards*, *118*, 1065–1083.

Tela, Y. T., Wassie, S. B., & Ferede, M. B. (2024). Assessment of meteorological and socioeconomic drought conditions in the Tekeze watershed, northern Ethiopia. *Frontiers in Environmental Science*, 12, 1506883.

The Nation Thailand. (2025). *24 Thai provinces on high alert for flooding, landslides, and flash floods from August 15-17.* https://www.nationthailand.com/news/general/40054028

United Nations General Assembly. (2016). *Report of the open-ended intergovernmental expert working group on indicators and terminology relating to disaster risk reduction*. United Nations.

Van Niekerk, D., Nemakonde, L. D., Kruger, L., & Genade, K. (2017). Community-based disaster risk management. In Rodríguez, H., Donner, W., & Trainor, J.E. (Eds.), *Handbook of disaster research* (pp. 411–429). Springer.

Waseem, M., Ahmad, S., Ahmad, I., Wahab, H., & Leta, M. K. (2023). Urban flood risk assessment using AHP and geospatial techniques in Swat, Pakistan. *SN Applied Sciences*, *5*, 215.

Weather Spark. (2025). *Climate and average weather year round at Tak Thailand*. https://weatherspark.com/y/149071/Average-Weather-at-Tak-Thailand

Yalcin, A. (2008). GIS-based landslide susceptibility mapping using analytical hierarchy process and bivariate statistics in Ardesen (Turkey): Comparisons of results and confirmations. *Catena*, *72*(1), 1–12.

Yesilnacar, E., & Topal, T. (2005). Landslide susceptibility mapping: A comparison of logistic regression and neural networks methods in a medium scale study, Hendek region (Turkey). *Engineering Geology*, *79*, 251–266.